RSC Advances

PAPER

View Article Online
View Journal | View Issue

Cite this: *RSC Adv.*, 2015, **5**, 9727

Synthesis of dual type Fe species supported mesostructured silica nanoparticles: synergistical effects in photocatalytic activity†

R. Jusoh,[a] A. A. Jalil,*[ab] S. Triwahyono[c] and N. H. N. Kamarudin[a]

Received 4th November 2014
Accepted 5th January 2015

DOI: 10.1039/c4ra13837f

www.rsc.org/advances

Dual type Fe species (isomorphously substituted Fe species and a colloidal α-FeOOH (IS-FeOOH)) supported on mesostructured silica nanoparticles (IS-FeOOH/MSN) were prepared by a simple electrochemical method followed by impregnation. Characterization was conducted using X-ray diffraction, transmission electron microscopy, surface area analysis, Fourier-transform infrared spectroscopy, nuclear magnetic resonance, electron spin resonance, and X-ray photoelectron spectroscopy. The results suggested that silica removal occurred in the MSN framework to isomorphously substitute Fe cations while retaining the colloidal structure of IS-FeOOH. The catalytic activity of IS-FeOOH/MSN was tested on photo-Fenton-like degradation of 2-chlorophenol under fluorescent light irradiation. The performance of the catalyst was in the following order: 10 wt% IS-FeOOH/MSN > 15 wt% IS-FeOOH/MSN > 5 wt% IS-FeOOH/MSN > MSN, with removal percentages of 92.2, 79.3, 73.1, and 14.2%, respectively. The results suggest that a synergistic effect between the dual type of Fe species (Si–O–Fe and IS-FeOOH colloid) and MSN played important roles in enhancing the degradation. The results provide strong evidence to support the potential use of IS-FeOOH/MSN as a photo-Fenton-like nanocatalyst for organic pollutants treatment.

1. Introduction

The presence of chlorinated compounds in aquatic environments such as 2-chlorophenol (2-CP), which is widely used in various chemical processes has caused severe environmental problems.[1] They present a serious threat to the surrounding ecosystem since chlorinated compounds are known to be the starting material for dioxins and furans.[2] Thus, an efficient treatment is required to avoid the environmental impact caused by these harmful pollutants. The integration of two different Advanced Oxidation Technologies (AOTs) (photocatalytic and Fenton-like) offers synergistic reaction routes for enhanced degradation efficiency of target wastewaters, which are suitable for the degradation of various chlorinated phenol pollutants.[3–5] However, the photo-Fenton-like catalysts generally face a practical problem, *i.e.*, the undesired electron–hole pair recombination that represents major energy-wasting step that may hinder the efficiency of the system.

α-FeOOH has been widely used as a semiconductor catalyst for degradation of many chlorinated compounds owing to its unique electrical, optical, and photoluminescence properties with a low band-gap energy (2.2 eV).[6,7] However, α-FeOOH nanoparticles have small surface areas that cause poor photocatalytic performances due to insufficient contact with the reactants.[8] Thus, a suitable method to improve the contact between pollutant molecules and a catalyst with low usage of metal oxide in the treatment system should be investigated. One method is an incorporation of the metal oxide onto mesoporous materials support, which has been discussed by several research groups in recent years.[9–11] For instance, mesostructured silica nanoparticles (MSN) is the most popular and has been considered as a potential solid support for heterogeneous catalysts.[12]

Recently, we have reported the effective use of modified MSN in drug delivery system, adsorption, isomerization, and photocatalysis,[13–18] which related to its distinctive properties such as ordered porous structure, high surface area (>1000 $m^2\ g^{-1}$), large pore volume, and tunable pore size (1.5–10 nm). On the other hand, we also reported a simple electrosynthesis of colloidal α-FeOOH nanoparticles in ionic surfactant (IS), which inhibited the electron–hole recombination to enhance the photodegradation of 2-CP.[19] However, the result is still low and beyond the industrial requirement. Therefore, incorporation of the colloidal metal onto a support material is very decisive. Although several studies have been conducted to deposit the

[a]*Department of Chemical Engineering, Faculty of Chemical Engineering, Universiti Teknologi Malaysia, 81310 UTM Johor Bahru, Johor, Malaysia. E-mail: aishah@cheme.utm.my*

[b]*Institute of Hydrogen Economy, Universiti Teknologi Malaysia, 81310 UTM Johor Bahru, Johor, Malaysia*

[c]*Department of Chemistry, Faculty of Science, Universiti Teknologi Malaysia, 81310 UTM Johor Bahru, Johor, Malaysia*

† Electronic supplementary information (ESI) available. See DOI: 10.1039/c4ra13837f

colloidal metal onto several supports including clay, metal oxide, and activated carbon,[20–22] the study on the interaction of electrosynthesized colloidal metal oxide on a mesostructured silica nanoparticles support is still rare. Moreover, the properties of the catalyst are known to be strongly affected by the support, which makes it very complicated to understand its reaction mechanism. Thus, detail investigation on supported colloidal metal catalyst is very crucial.

Therefore, herein we report a synthesis of IS-FeOOH supported on MSN in order to enhance the surface contact for an efficient photodegradation. The physicochemical properties of the IS-FeOOH/MSN were studied in detail to clarify its structure. Remarkably, it was found that besides the retainment of IS-FeOOH colloidal structure, the isomorphously substituted Fe species was also formed. This dual types Fe species are synergically performed with MSN support to significantly give almost complete photo-degradation of 2-CP.

2. Experimental

2.1 Materials

2-CP Alfa Aesar® (99% purity) was used without further purification. Mono-cationic ionic surfactant (IS), dodecyltrimethylammonium bromide was purchased from Fisher Scientific, Malaysia. Iron and platinum plates (>99.99% purity) were obtained from Nilaco, Japan. CH_3OH, NaOH and HCl were obtained from HmbG Chemicals, Malaysia. Cetyltrimethylammonium bromide (CTAB), ethylene glycol (EG), and tetraethyl orthosilicate (TEOS) were purchased from Merck, Malaysia. Ammonium hydroxide solution (NH_4OH) was obtained from QRec, Malaysia. Deionized water supplied by the Bibby Sterilin Ltd, UK water treatment system was used to prepare all the solutions.

2.2 Catalyst preparation

MSN were prepared by sol–gel method.[14] The CTAB, EG, and NH_4OH solution were dissolved in 700 mL water with following mole composition, respectively: 0.0032 : 0.2 : 0.2 : 0.1. After 30 min vigorous stirring with heating, 1.2 mmol TEOS were added to give a white suspension solution. This solution was stirred for another 2 h, followed by centrifugation, drying at 333 K and calcined at 823 K for 3 h.

The synthesis procedure of α-FeOOH nanoparticles were similar to those reported in literature.[15,16,19] 15 mL IS/water solution, with IS to water of 1 : 1 volume ratio was added to one-compartment cell equipped with magnetic stirring bar and a two-electrode configuration of an iron plate (2 cm × 2 cm) anode and a platinum plate (2 cm × 2 cm) cathode. Electrolysis was conducted at a constant current of 60 mA cm^{-2} and 273 K under air atmosphere. The weight percentage of IS-FeOOH supported on MSN was calculated by the time of electrolysis, which is based on the Faraday's law (eqn (1)),

$$t = \left(\frac{F}{I}\right)(z \times n) \quad (1)$$

where t is the total time for the constant current applied (s); F is the 96 486 C mol^{-1}, which is the Faraday constant; I is the electric current applied (mA); z is the valency number of ions of substance (electrons transferred per ion); and n is the number of moles of substance (number of moles, liberated $n = m\ M^{-1}$). After electrolysis of prescribe weight percentage of IS-FeOOH, the corresponding mixture was impregnated to MSN at 353 K to give a series of IS-FeOOH/MSN.

2.3 Characterization

Crystallinity study was recorded on D8 ADVANCE Bruker X-ray diffractometer using Cu Kα radiation at 2θ (2° to 90°). Joint Committee on Powder Diffraction Standards (JCPDS) files was used to identify the phases. Morphology of MSN with the distribution of IS-FeOOH was examined by TEM (JEOL JEM-2100F).

Surface area of IS-FeOOH/MSN was calculated with Brunnauer–Emmett–Teller (BET) method using a Micromeritics ASAP 2010 instrument. The functional groups of IS-FeOOH/MSN were identified using an Agilent Cary 640 Fourier-transform infrared (FT-IR) Spectrometer using the KBr method with a scan range of 400–4000 cm^{-1}.

^{29}Si MAS NMR spectra were recorded on a Bruker Advance 400 MHz 9.4 T spectrometer at frequency of 104.2 MHz and 79.4 MHz, respectively. A JEOL JES-FA100 ESR spectrometer was used to observe the formation of electron–holes or unpaired electrons at room temperature. Chemical oxidation state of the IS-FeOOH/MSN catalyst was determined using XPS conducted on a Kratos Ultra spectrometer equipped with a Mg Kα radiation source (10 mA, 15 kV) in the range of 0–800 eV. Photoluminescence (PL) (JASCO Spectrofluorometer) (FP-8500) with 150 W Xe lamp as excitation source were employed to study the electronic structure, optical and photochemical properties of semiconductor.

The analysis regarding the optical absorption properties of the catalysts were obtained using a PerkinElmer UV-vis/DRS Spectrophotometer in the range of 200–800 nm at room temperature. The band gap of catalysts was determined from plots of the Kubelka–Munk (K–M) function $[f_{K-M} = (h\nu/\lambda)^{1/2}]$ as a function of the energy of the excitation light $[h\nu]$.

2.4 Catalytic testing

Catalytic activity was tested on a photo-Fenton-like degradation of 2-CP. Catalyst (0.400 g L^{-1}) was added to 50 mg L^{-1} 2-CP solution in a Pyrex batch photoreactor, 140 mm length and 85 mm diameter with a total volume of 0.25 m^3 and was stirred for 2 h in the dark to achieve adsorption–desorption equilibrium with a stirring rate of 250 rpm. Philips TL 20W/52 fluorescent lamp within quartz glass housing (emission spectrum 350–600 nm) with a peak emission at 430 nm was employed as the light source. It was found that the fluorescent lamp emitted ultraviolet-visible (UV-Vis) radiation consists of visible light, UV-A, and UV-B radiation, with highest light emission of visible radiation.[23]

The entire set-up was placed inside a chamber covered with aluminium foil to prevent the passage of other lights. Initial pH

of the solution was 5 and the reaction was carried out at 303 K. Then 0.156 mM hydrogen peroxide (H_2O_2) was added and ambient air was bubbled into the system continuously using an air pump (AC 100–240 V, 12 W motor) before the reaction was performed for another 8 h under UV-Vis light irradiation. During the reaction, aliquots of 2 mL were taken out at 15 min intervals and centrifuged in a Hettich Zentrifugen Micro 120 at 75 000 rpm for 10 min before analysis by a double-beam UV-Vis spectrophotometer (Cary 60 UV-Vis Agilent) at 274 nm. All experiments were performed in triplicate; error bars represent standard error of the mean.

3. Results and discussion

3.1 Crystallinity, phase, and structural studies

Fig. 1 shows the XRD patterns of IS-FeOOH, MSN, and IS-FeOOH/MSN catalysts with different IS-FeOOH loading. The nanoparticles collected from the electrolysis cell (IS-FeOOH) showed diffraction peaks of pure orthorhombic phase of α-FeOOH (Fig. 1A). The *d*-spacing observed for the strong (110) facet was identical to the literature (0.418 nm).[24] For IS-FeOOH loaded MSN, three main diffraction peaks indexed as (100), (110), and (200) reflections were observed, which corresponded to *p6mm* hexagonal symmetry in the mesostructured silica[13] (Fig. 1B). Introduction of IS-FeOOH onto MSN inhibit the formation of the (100) peak, while the other two peaks were almost eliminated, signifying slight loss in MSN hexagonal structure ordering.[25] The absence of IS-FeOOH diffraction peaks in IS-FeOOH/MSN may be due to the very small number of α-FeOOH species that are undetectable with XRD.[26]

3.2 Morphological properties

Morphological properties of MSN and IS-FeOOH/MSN were examined by TEM as presented in Fig. 2. Fig. 2A shows a well-defined mesostructured nanoparticles and ordered pores of MSN. Introduction of IS-FeOOH onto MSN did not alter the original morphology and IS-FeOOH was observed to be well deposited on the MSN surface (Fig. 2B).

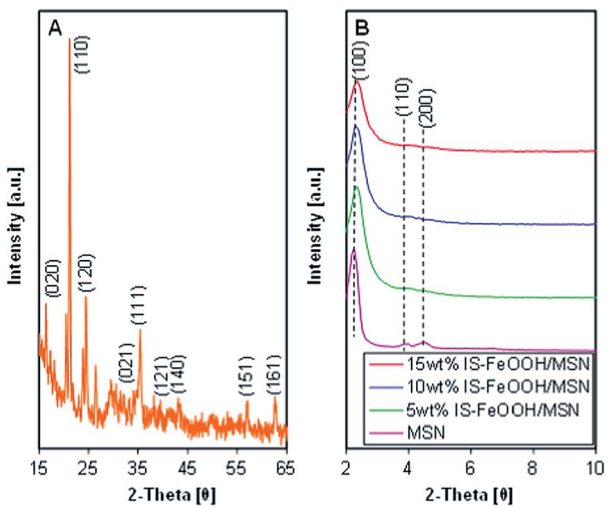

Fig. 1 XRD patterns of catalysts. (A) Region 15–65° of IS-FeOOH; (B) region 2–10° of MSN and IS-FeOOH/MSN.

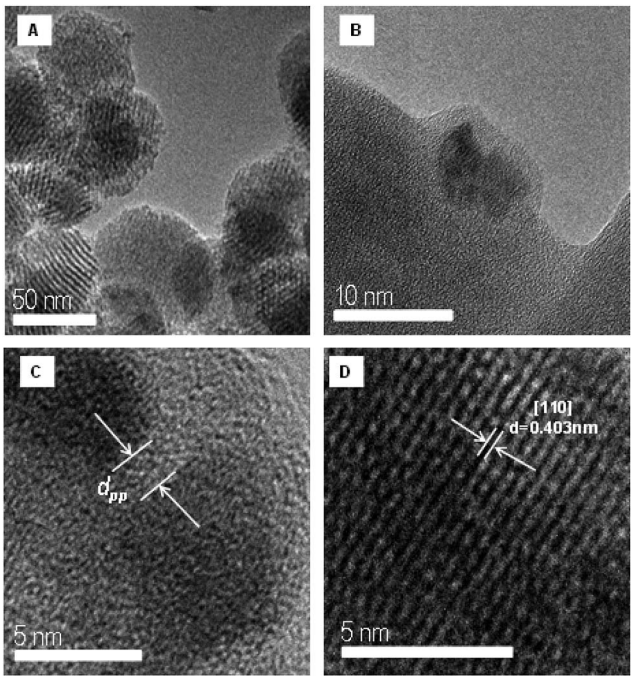

Fig. 2 TEM image of (A) MSN; (B and C) 10 wt% IS-FeOOH/MSN; (D) HRTEM image of 10 wt% IS-FeOOH/MSN.

Insight at higher magnification (Fig. 2C) showed that the deposited IS-FeOOH did not fuse into larger particles and retained its original particle size (5–10 nm) (ESI Fig. S1†), signifying a high stability even after introduction onto the MSN support. The average particle-to-particle distance (d_{pp}) measured was 2 ± 0.5 nm, shorter than twice the length of the IS molecule, which is 3.6 nm. This may suggest a retained colloidal structure around the α-FeOOH on the MSN support.[27] The value of the interplanar distance (*d*-spacing) of the lattice fringes estimated from the magnification of a selected area was 0.403 nm and it was consistent with the value of lattice spacing of IS-FeOOH obtained from the XRD analysis at (110) facet (Fig. 2D).

3.3 Surface area analysis

Porosity of the catalyst was studied by the pore size distributions depicted in Fig. 3. MSN showed bimodal pore size distributions that consisted of a primary pore at 2.7 ± 0.9 nm and secondary pore at 3.5 ± 0.7 nm. Introduction of IS-FeOOH onto MSN has successfully retained its bimodal structures, with decreasing in the intrapore and increase in the interpore distribution. However, loading of larger amount of IS-FeOOH onto MSN induced pore blockage, which subsequently reduced the pore volume of 10 and 15% IS-FeOOH/MSN compared with 5% IS-FeOOH/MSN.

As shown in Table 1, surface area (S_{BET}) of IS-FeOOH/MSN decreased from 1107 to 665 $m^2\ g^{-1}$, following the order MSN > 5 wt% IS-FeOOH/MSN > 10 wt% IS-FeOOH/MSN > 15 wt% IS-FeOOH/MSN. This suggested that a portion of the IS-FeOOH

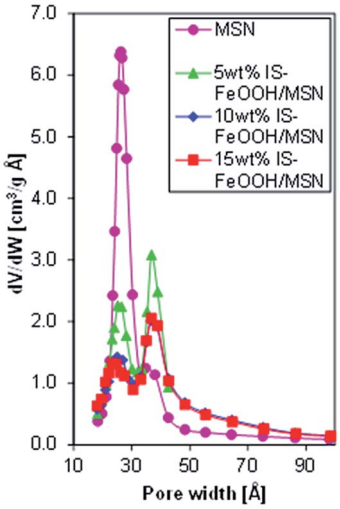

Fig. 3 Pore distribution of catalysts.

was dispersed on the surface of MSN. Average pore size of MSN was found to be increased upon the introduction of IS-FeOOH, that might be due to the increase in interparticle pores, as shown in Fig. 3. Indeed, formation of a bimodal pore structure may be related to the removal of silica from MSN framework.[28] Increasing the amount of IS-FeOOH loaded may induce the silica removal rate, which then led to the reduction in pore size and increase in pore volume of the MSN.[29]

3.4 Vibrational spectroscopy

All IS-FeOOH/MSNs were characterized by FTIR spectroscopy to verify the bonding between IS-FeOOH and MSN (Fig. 4). A broad band at 3421 cm^{-1} was observed, which could be attributed to the stretching vibrations of the hydroxyl group (Fig. 4A).[14] The CH_2 stretching vibrations of IS at band 2927 and 2850 cm^{-1} were observed for all IS-FeOOH/MSN samples, indicating the presence of colloidal IS-FeOOH in the IS-FeOOH/MSNs.

Fig. 4B shows a broad band at 1621 cm^{-1} in all samples, which attributed to the bending vibration of the OH group for both IS-FeOOH and MSN.[30] Doublet peaks observed at band 1480 and 1465 cm^{-1} in the IS-FeOOH spectrum correspond to the CH_2 scissoring mode of the IS methylene chain.[31] These bands were significantly observed in IS-FeOOH/MSNs, suggesting the presence of colloidal IS-FeOOH. The peak at 1430 cm^{-1}, which corresponds to head group vibrations of the IS, was observed for all samples.[19] This implies that the interaction of N^+ with IS-FeOOH is retained for all samples.

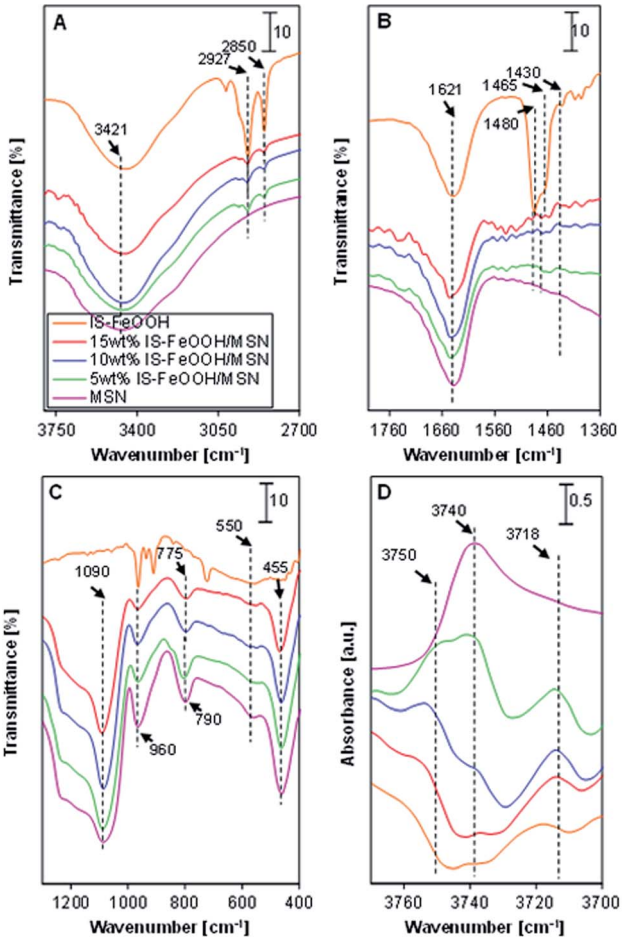

Fig. 4 FT-IR spectra of catalysts. (A) Region 3800–2700 cm^{-1}; (B) region 1800–1360 cm^{-1}; (C) region 1300–400 cm^{-1}; (D) in evacuated system for region 3770–3700 cm^{-1}.

The bands at 1090, 790, and 455 cm^{-1} for MSN and IS-FeOOH/MSN catalysts shown in Fig. 4C are attributed to the characteristics of the silica structure of asymmetric stretching, symmetric stretching, and bending vibration of Si–O–Si bonds, respectively.[32] The introduction of IS-FeOOH species onto MSN decreased the intensity of all bands, implying a perturbation of silica network due to removal of silica. Meanwhile, the slight shift of the 790 cm^{-1} band to 775 cm^{-1} may be attributed to the vibration of Fe^{3+}–OH, which illustrates the formation of OH layer around the metal core.[33] The vibrational mode at around 960 cm^{-1} is attributed to silanol groups present at "defective

Table 1 Textural properties of catalysts

Sample	Surface area, S_{BET} (m^2 g^{-1})	Average pore size, D_{pore} (nm)	Average pore volume, V_{pore} (cm^3 g^{-1})
MSN	1107	3.00 ± 1.20	2.14
5 wt% IS-FeOOH/MSN	850	3.10 ± 1.14	0.61
10 wt% IS-FeOOH/MSN	734	3.09 ± 1.27	1.04
15 wt% IS-FeOOH/MSN	665	3.01 ± 1.19	0.99

sites".[32] The decrease of this band with increasing IS-FeOOH loading also signifies its possible interaction with Fe species. Furthermore, the band at 550 cm^{-1}, which corresponds to Si–O bond,[34] was also decreased with increasing IS-FeOOH loading, indicating significant interaction of silica framework with Fe species from IS-FeOOH.

For further investigation of IS-FeOOH/MSN structural properties, the catalysts were evacuated for 1 h at 623 K prior to IR measurement to remove the physisorbed water. In Fig. 4D, a new band at 3750 cm^{-1} appeared in all IS-FeOOH/MSN samples which attributed to the germinal silanol groups.[35] The band at 3740 cm^{-1}, which is ascribed to the terminal silanol groups[36] decreased with increasing IS-FeOOH loading, which confirmed the perturbation of silica framework. Meanwhile, the band at 3718 cm^{-1} which is assigned to hydroxyl nests,[37] decreased with increasing IS-FeOOH loading. Thus, the results suggested that introduction of IS-FeOOH onto the MSN caused silica removal in the silica framework. It was also found that the colloidal IS-FeOOH still retain its structure after its loading onto MSN. These may due to the strong binding of IS molecules to the IS-FeOOH nanoparticles which hinder other binding displacement to its surface.[38] In a mean time, the colloidal IS-FeOOH may adsorbed to the MSN surface which induced the attachment of colloidal IS-FeOOH onto the MSN support.[39]

Meanwhile, in order to investigate the bonding of MSN framework with the Fe species, the overlapped band at 960 cm^{-1} was also further confirmed by a Gaussian curve-fitting as shown in ESI (Fig. S2†). Significantly, a new band was observed at 955 cm^{-1} when 5 wt% IS-FeOOH was added onto the MSN, which correspond to Si–O–Fe stretching vibrations.[32] The band increased by increasing IS-FeOOH loading up to 10 wt%, which confirmed the isomorphous substitution of Fe species after the removal of silica from MSN framework. This Fe species may be originated from the abundant Fe^{3+} ions in electrolysis cell which have not yet transformed to IS-FeOOH. However, the increase of IS-FeOOH loading up to 15 wt% showed no further increase in the band. This may be due to the saturation of Fe species–MSN interactions. The result also illustrated that the isomorphously substituted Fe species was not from the bulky colloidal structure of IS-FeOOH.

3.5 Nuclear magnetic resonance (NMR)

The MSN and 10 wt% IS-FeOOH/MSN was subjected to ^{29}Si MAS NMR to compare and elucidate their detailed structure (Fig. 5A). The dominant signal shown by MSN at approximately −112.485 ppm was assigned to $(\equiv SiO)_4Si$. This peak reduced and shifted to −105.110 by the loading of IS-FeOOH, indicating the alteration at $(\equiv SiO)_4Si$ sites.

New shoulders were developed in the range of −80 to −90 ppm and −90 to −100 ppm, which signified that the $(\equiv SiO)_2Si$ and $(\equiv SiO)_3Si$ sites were formed in consequence of silica removal in MSN framework.[26] This result is consistent with XRD and FTIR, which support the decreased of Si–O–Si bonds. In fact, the silica removal that occurred may be due to the presence of ammonium salt in the synthesis process.[40] The interaction between ammonium ions and silica followed by subsequent attack of the hydroxide ions on the external surface of MSN may dissociate some Si–O–Si bonds from the framework.

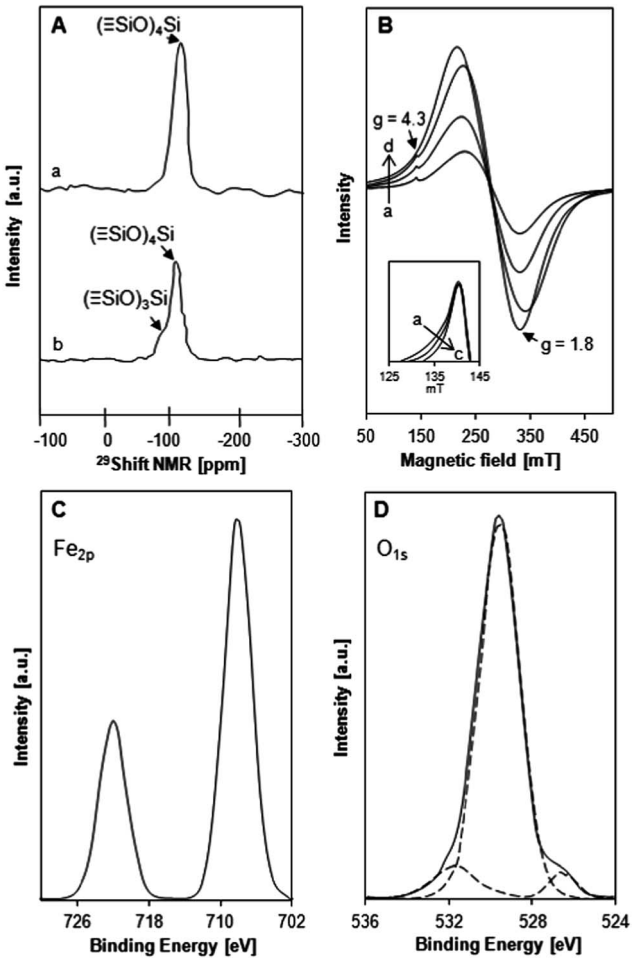

Fig. 5 (A) ^{29}Si MAS NMR spectra of (a) MSN and (b) 10 wt% IS-FeOOH/MSN; (B) ESR spectra of (a) 5 wt% IS-FeOOH/MSN, (b) 10 wt% IS-FeOOH/MSN, (c) 15 wt% IS-FeOOH/MSN, and (d) IS-FeOOH; XPS spectra of (B) Fe_{2p} and (C) Si_{2p} for 10 wt% IS-FeOOH/MSN catalyst.

3.6 Chemical oxidation state determination

The ESR spectroscopy is a very sensitive technique for studying the nature and the crystal symmetry environment of iron in mesoporous silica. Thus, the IS-FeOOH and IS-FeOOH/MSN catalysts were subjected to ESR and the spectra are presented in Fig. 5B. The presence of a signal at $g = 4.3$ for all IS-FeOOH/MSN samples indicate the presence of Fe^{3+} in the MSN framework.[41] This observation is in agreement with the FTIR results, which suggest free Fe species might take part in the isomorphous substitution step, which indicates that two types of iron are present in the IS-FeOOH/MSN catalyst structure. The normalization of peak at $g = 4.3$ (inset figure) indicates that all IS-FeOOH/MSN samples have different bandwidth which suggest different arrangement of Fe^{3+} in the MSN framework.[42] This is also in agreement with the FTIR result which suggests gradual silica removal step accompanied with isomorphous substitution of Fe cations at different IS-FeOOH loading onto

MSN. The $g = 1.8$ was also observed for all samples which attributes to the presence of organometallic, signifying the IS-FeOOH is retained in the MSN framework.[43] Both signals show pronounced shifts after IS-FeOOH were loaded onto MSN, which confirm the bonding of Fe species and colloidal IS-FeOOH with the MSN support.

The 10 wt% IS-FeOOH/MSN catalyst was then subjected to XPS analysis in order to elucidate its exact structure. The Fe_{2p} doublet with binding energies of 708 and 722 eV shown in Fig. 5C implied the presence of Fe–O bond of the IS-FeOOH species.[44] Meanwhile, the three peaks at 527, 530, and 533 eV displayed by the O_{1s} (Fig. 5D) correspond to the presence of Si–O–Si, Si–O–Fe and Si–O–H bonds, respectively, since the binding energy of electrons at the oxygen atom increases as the electron–electron repulsion decreases due to the electronegativity sequence of its adjacent atom: hydrogen > iron > silica.[45] Therefore, it was confirmed that Si–O–Fe groups were present in the IS-FeOOH/MSN catalyst and this was in agreement with FTIR results.

3.7 Proposed structure of IS-FeOOH/MSN

Based on the above characterization results, a probable IS-FeOOH/MSN structure is proposed as shown in Fig. 6. The presence of IS ammonium groups in IS-FeOOH/MSN system during the preparation step caused removal of silica, which then induced the isomorphous substitution of free Fe^{3+} species in the system, as proven by the presence of Si–O–Fe bond in FTIR and XPS data.[28] The XRD, surface area analyses, and NMR also supported the silica removal process. The colloidal form of IS-FeOOH was also found to be retained and dispersed well on the MSN support as verified by the TEM and FTIR results.[19] The decrease in intraparticle pores and simultaneous increase in interparticle pores with increasing IS-FeOOH/MSN loading, as shown by the pore size distribution result, as well as the ESR results, also clarified the isomorphous substitution of Fe^{3+} species and the retainment of colloidal IS-FeOOH structure on the MSN. Remarkably, the results show that two types of Fe species could be formed when using MSN as a support in the IS system.

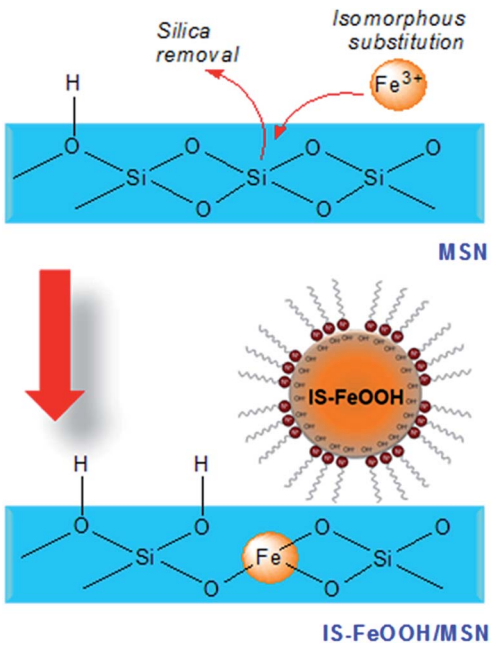

Fig. 6 Proposed structure of IS-FeOOH/MSN.

3.8 Photo-Fenton-like performance of IS-FeOOH/MSNs

The performance of IS-FeOOH/MSN was examined for photodegradation of 2-CP under UV-Vis light conditions. The results are shown in Fig. 7A. Only 14.2% of the 2-CP was removed when using the bare MSN, most probably due to the generated $^{\bullet}OH$ *via* direct photoconversion of the added H_2O_2. Meanwhile, 64.3% of the 2-CP was degraded when using the pristine IS-FeOOH under the same conditions. The removal percentage were increased up to 73.1% and 92.2% by using the 5 wt% IS-FeOOH/MSN and 10 wt% IS-FeOOH/MSN, respectively. Proper distribution of IS-FeOOH nanoparticles on the surface of MSN might facilitate their surface contact with light, which led to higher efficiency of degradation.[16] In contrast, further increase in IS-FeOOH/MSN loading give no significant effect on the degradation. Fig. 7B shows the photodegradation rate constant as a function of IS-FeOOH loading. It can be seen that 10 wt% IS-FeOOH/MSN gave the highest rate constant of 3.2×10^{-3} min^{-1}, followed by the 15 wt% and 5 wt% IS-FeOOH/MSN, with rate constants of 3.1×10^{-3} min^{-1} and 2.7×10^{-3} min^{-1}, respectively.

The IS-FeOOH/MSN catalysts were also subjected to photoluminescence (PL) analysis at an excitation wavelength of 650 nm in visible region (Fig. 8). 5 wt% IS-FeOOH/MSN showed highest peak intensity, followed by the 15 wt% and 10 wt% IS-FeOOH/MSN. Addition of IS-FeOOH decreased the content of surface oxygen vacancies and/or defect sites, which affected the intensity and response range of PL signals.[46] Indeed, the oxygen vacancies and defect sites are important to trap the electrons to keep the e^-–h^+ pairs separate in order to enhance photocatalytic activity. It has been reported that the lower the peak intensity, the lower the recombination rate of the photoinduced electron–hole pair, which results in higher photocatalytic activity.[15] This fact may explain why the photocatalytic activity was in the following order: 10 wt% IS-FeOOH/MSN > 15 wt% IS-FeOOH/MSN > 5 wt% IS-FeOOH/MSN. The limitation of increasing IS-FeOOH loading to 15 wt% may be because of the accumulation of excess IS-FeOOH on the surface of the IS-FeOOH/MSN catalysts, which led to the lower rate constant and photoactivity.[41]

This result is in agreement with the band gap determination results shown in Table 2. The band gap energy of IS-FeOOH and IS-FeOOH/MSNs was determined using Kubelka–Munk (K–M) spectrum. The results show a reduction in band gap energy with increase in IS-FeOOH loading up to 15 wt%. It was known that low band gap energy results in efficient performance of photocatalyst. However, the aforementioned possibility of the IS-FeOOH accumulation on 15 wt% IS-FeOOH/MSN surface may hinder its effective performance towards the 2-CP degradation, regardless of the low band gap energy value.

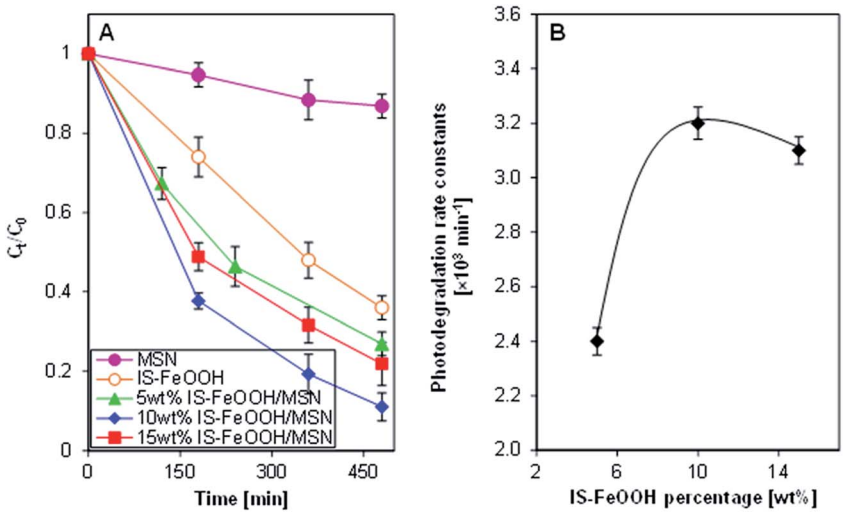

Fig. 7 (A) The 2-CP photodegradation performance; (B) the degradation rate constants of the catalysts against the IS-FeOOH percentage in MSN [pH 5; H_2O_2 concentration is 0.156 mM, catalyst dosage 0.40 g L^{-1}; initial concentration is 50 mg L^{-1}].

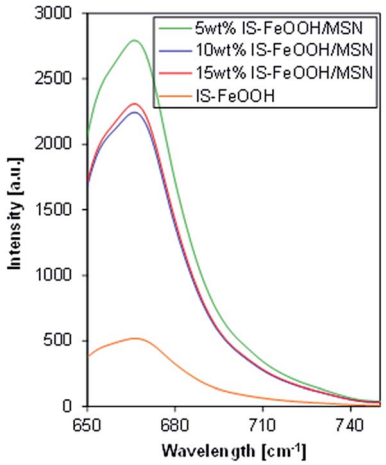

Fig. 8 Photoluminescence spectra for IS-FeOOH/MSN catalysts.

Table 2 Calculated band gap value for each catalyst

Catalysts	Band gap[a] (eV)
IS-FeOOH	2.75
5 wt% IS-FeOOH/MSN	3.25
10 wt% IS-FeOOH/MSN	3.00
15 wt% IS-FeOOH/MSN	2.90

[a] Derived from plotted graph K–M *versus hv*.

3.9 Proposed 2-CP degradation mechanism by IS-FeOOH/MSN

Next, with the purpose of investigating the mechanism of 2-CP degradation *via* IS-FeOOH/MSN, the effect of scavenging agents was studied by using 10 wt% IS-FeOOH/MSN. Four types of scavengers were used for the system: potassium dichromate (PD); isopropanol (IP); sodium oxalate (SO); and potassium iodide (PI), with the role as a scavenger of photogenerated electrons, hydroxyl radicals ($^{\bullet}OH$), photogenerated holes (H^+), and hydroxyl radicals adsorbed on the catalyst surface ($^{\bullet}OH_{ads}$), respectively. The PD scavenger may also provide indirect sight to the presence of superoxide anion ($^{\bullet}O_2^-$) in the system since PD is an effective quencher to indicates the reactive species on the reduction pathways, including both photogenerated electrons and $^{\bullet}O_2^-$.[47] Furthermore, due to the reported fate of short-lived $^{\bullet}O_2^-$ radicals in water and the transition from $^{\bullet}O_2^-$ to $^{\bullet}OH$ was estimated to be too fast to be detected,[48] this study focus on one of the species in the reduction pathways, which is the photogenerated electron.

Fig. 9A shows that PD reduced the degradation efficiency to 59%. The addition of IP and PI decreased the 2-CP degradation efficiency to 16% and 18%, respectively, while the addition of SO fully inhibited the degradation efficiency, confirming that photogenerated hole was the main oxidation species for degrading 2-CP and significantly assisted by hydroxyl radicals ($^{\bullet}OH$) and hydroxyl radicals adsorbed on the catalyst surface ($^{\bullet}OH_{ads}$).

As proposed in Fig. 9B, both type of the iron species played role in the photocatalytic process. The IS-FeOOH could trap the photogenerated electron by the colloidal structure around the IS-FeOOH. Meanwhile, the substituted Fe species may inhibit the electron–hole recombination by transferring the photoinduced electron to the support as MSN could also acts as stable electron acceptors.[49]

As proven by SO, the photogenerated holes (h^+_{VB}) at the valence band, which have high oxidation potential, play two important roles in this degradation. Firstly, they permit the direct oxidation of 2-CP to reactive intermediates (eqn (2)):

$$\text{2-CP} + h^+_{VB} \rightarrow \text{oxidation of 2-CP} \quad (2)$$

Secondly, h^+_{VB} also react with surface-adsorbed hydroxyl groups (OH^-) or water to yield surface-adsorbed hydroxyl radicals ($^{\bullet}OH_{ads}$), which subsequently degrade the 2-CP, as shown by the decrease in degradation efficiency by PI[47] (eqn (3)):

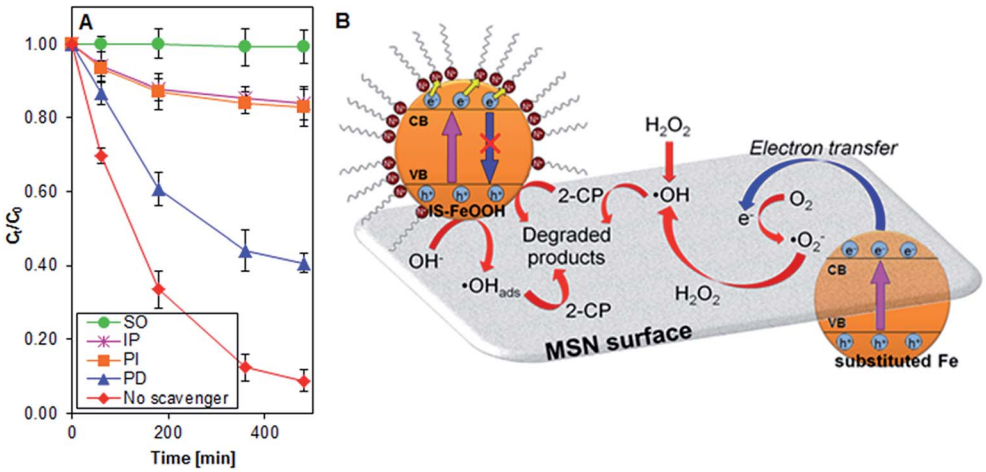

Fig. 9 (A) Photodegradation efficiencies of 2-CP in the presence of hole scavenger, •OH scavenger, electron scavenger, and $•OH_{ads}$ scavenger by 10 wt% IS-FeOOH/MSN catalyst [pH 5; H_2O_2 concentration is 0.156 mM, catalyst dosage 0.40 g L^{-1}; initial concentration is 50 mg L^{-1}]; (B) schematic illustration of 2-CP photodegradation over IS-FeOOH/MSN.

$$OH^- + h^+_{VB} \rightarrow •OH_{ads} \quad (3)$$

The addition of IP showed a rather lower degradation percentage, indicating a significant role of •OH in the system. In fact, •OH could be generated *via* direct photoconversion of H_2O_2 (eqn (4)) or by photogenerated electron-induced multistep reduction of O_2 (eqn (5)–(7)) to degrade the 2-CP:[50]

$$H_2O_2 \xrightarrow{h\nu} 2•OH \quad (4)$$

$$O_2 + e^- \rightarrow •O_2^- \quad (5)$$

$$•O_2^- + e^- + 2H^+ \rightarrow H_2O_2 \quad (6)$$

$$H_2O_2 + e^- \rightarrow OH^- + •OH \quad (7)$$

In the case of PD, although the photo-induced electrons at the conduction band have been captured by PD, •OH could still be produced by direct photoconversion of H_2O_2 (eqn (4)). Therefore, this mechanism demonstrates the significant role of the silica support as an acceptor of photo-induced electrons to efficiently inhibit the recombination of electron–hole pairs that leads to enhanced degradation of 2-CP.

3.10 Reusability study

Repeated experiments were carried out using 10 wt% IS-FeOOH/MSN in order to study the stability of the catalyst for the degradation of 2-CP (Fig. 10). It can be observed that after four repeated cycles, the catalyst was still active with just a small decrease in 2-CP degradation percentage from 92% to 87%. However, a relatively significant decrease of degradation was observed after the fifth cycle (83%). The results suggest gradual detachment of the colloidal formation on the IS-FeOOH after fifth cycles. In addition, the bonding of the adsorped pollutant

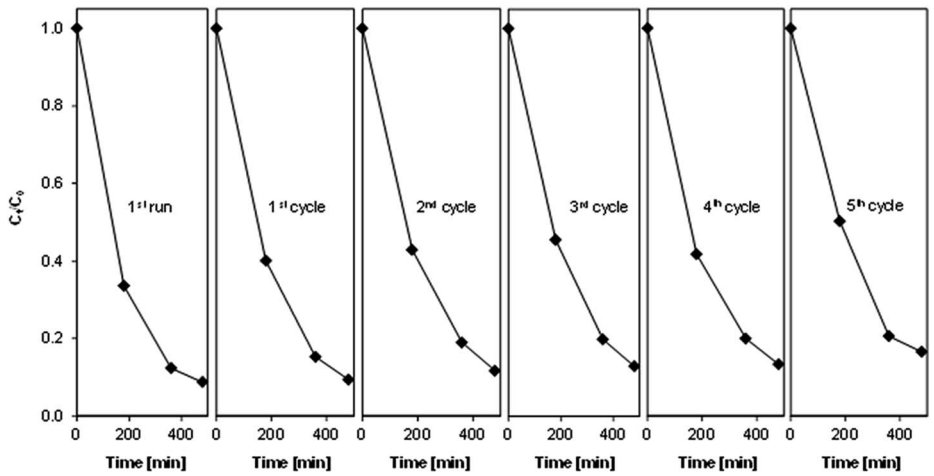

Fig. 10 Stability of 10 wt% IS-FeOOH/MSN catalyst after subsequent reactions [pH 5; H_2O_2 concentration is 0.156 mM, catalyst dosage 0.40 g L^{-1}; initial concentration is 50 mg L^{-1}].

onto the support material may hinder the availability of active sites, which therefore reduced the 2-CP degradation efficiency.

4. Conclusions

In this study, IS-FeOOH/MSN catalysts were prepared and used in an enhanced photo-Fenton-like degradation of 2-cholorophenol.[3,4] This study report the utilization of IS for the electrosynthesis of metal oxide followed by impregnation onto a silica support material, which may provide new insight to the previously reported study on IS-modified silica support.[51] It is clearly observed from FTIR, NMR, XPS, ESR and surface area analysis that the introduction of IS-FeOOH onto MSN significantly induced the silica removal followed by isomorphous substitution of free Fe species. The characterization results also verified the retention of IS-FeOOH colloidal formation even after being loaded onto MSN.

The performance of IS-FeOOH/MSN was investigated for 2-CP UV-Vis light degradation. Previous report on the supported colloidal metal indicates that the presence of ionic surfactant in the catalyst system decreased the catalyst activity for gas-phase reaction.[39] This study, however, indicates that the retention of colloidal metal over MSN support could trap the photo-generated electron. In the meantime, the substituted Fe species (Si–O–Fe) may inhibit the electron–hole recombination by transferring the photoinduced electron to the MSN support.[49] The synergic effect between the dual types Fe species with the MSN was able to occur in regards to the support material that acts as a stable electron acceptor. The stability test shows that the IS-FeOOH/MSN catalyst is stable up to five cycles. Ferroudj and his co-workers has synthesized similar catalyst which is a maghemite iron supported on a silica and was shown to remarkably degrade dyes and nitrophenol.[52] Meanwhile, a catalyst consists of iron species and MCM-41 as a support material was synthesized by Li and co-workers for desulfurization of dibenzothiphene.[41] Both Ferroudj *et al.* and Li *et al.* reported high stability upon catalyst reusability up to 5 and 4 cycles, respectively, which is comparable with the reusability result of the catalyst in this study. It is believed that these IS-FeOOH/MSN catalysts may provide assistance in the development of colloidal properties in solid catalysts for various applications.

Acknowledgements

The authors are grateful for the financial support from Research University Grant Universiti Teknologi Malaysia (Grant no. 4L112), the Exploration Research Grant Scheme from Ministry of Higher Education Malaysia, the awards of the King's Scholarship and Fellowship Scheme from Universiti Malaysia Pahang (Rohayu Jusoh), and the Hitachi Scholarship Foundation.

References

1 N. C. Tolosa, M.-C. Lu, H. D. Mendoza and A. P. Rollon, *Appl. Catal., A*, 2011, **401**, 233.
2 A. A. Jalil, S. Triwahyono, N. A. M. Razali, N. H. H. Hairom, A. Idris, M. N. M. Muhid, A. Ismail, N. M. N. Yahaya, N. A. L. Ahmad and H. Dzinun, *J. Hazard. Mater.*, 2010, **174**, 581.
3 M. Munoz, Z. M. de Pedro, J. A. Casas and J. J. Rodriguez, *J. Hazard. Mater.*, 2011, **190**, 993.
4 M. Bertelli and E. Selli, *J. Hazard. Mater.*, 2006, **138**, 46.
5 A. Karci, I. Arslan-Alaton, T. Olmez-Hanci and M. Bekbölet, *J. Photochem. Photobiol., A*, 2012, **230**, 65.
6 A. Gajović, A. M. T. Silva, R. A. Segundo, S. Šturm, B. Jančar and M. Čeh, *Appl. Catal., B*, 2011, **103**, 351.
7 B. Gao, L. Liu, J. Liu and F. Yang, *Appl. Catal., B*, 2014, **147**, 929.
8 S. Anandan, A. Vinu, N. Venkatachalam, B. Arabindoo and V. Murugesan, *J. Mol. Catal. A: Chem.*, 2006, **256**, 312.
9 M. U. A. Prathap, B. Kaur and R. Srivastava, *J. Colloid Interface Sci.*, 2012, **381**, 143.
10 K. Niu, D. Shi, W. Dong, M. Chen and Z. Ni, *J. Colloid Interface Sci.*, 2011, **362**, 74.
11 C. Bouvy, W. Marine and B.-L. Su, *Chem. Phys. Lett.*, 2007, **438**, 67.
12 M. A. A. Aziz, A. A. Jalil, S. Triwahyono, R. R. Mukti, Y. H. Taufiq-Yap and M. R. Sazegar, *Appl. Catal., B*, 2014, **147**, 359.
13 N. H. N. Kamarudin, A. A. Jalil, S. Triwahyono, V. Artika, N. F. M. Salleh, A. H. Karim, N. F. Jaafar, M. R. Sazegar, R. R. Mukti, B. H. Hameed and A. Johari, *J. Colloid Interface Sci.*, 2014, **421**, 6.
14 A. H. Karim, A. A. Jalil, S. Triwahyono, S. M. Sidik, N. H. N. Kamarudin, R. Jusoh, N. W. C. Jusoh and B. H. Hameed, *J. Colloid Interface Sci.*, 2012, **386**, 307.
15 N. W. C. Jusoh, A. A. Jalil, S. Triwahyono, H. D. Setiabudi, N. Sapawe, M. A. H. Satar, A. H. Karim, N. H. N. Kamarudin, R. Jusoh, N. F. Jaafar, N. Salamun and J. Efendi, *Appl. Catal., A*, 2013, **468**, 276.
16 N. Sapawe, A. A. Jalil, S. Triwahyono, S. H. Adam, N. F. Jaafar and M. A. H. Satar, *Appl. Catal., B*, 2012, **125**, 311.
17 N. Sapawe, A. A. Jalil, S. Triwahyono, R. N. R. A. Sah, N. W. C. Jusoh, N. H. H. Hairom and J. Efendi, *Appl. Catal., A*, 2013, **456**, 144.
18 S. Triwahyono, A. A. Jalil, R. R. Mukti, M. Musthofa, N. A. M. Razali and M. A. A. Aziz, *Appl. Catal., A*, 2011, **407**, 91.
19 R. Jusoh, A. A. Jalil, S. Triwahyono, A. Idris, S. Haron, N. Sapawe, N. F. Jaafar and N. W. C. Jusoh, *Appl. Catal., A*, 2014, **469**, 33.
20 A. Mastalir, Z. Kiraly, G. Szollosi and M. Bartok, *Appl. Catal., A*, 2001, **213**, 133.
21 H. Sato, T. Ohtsu and I. Komazawa, *J. Chem. Eng. Jpn.*, 2002, **35**, 255.
22 F. Porta, L. Prati, M. Rossi and G. Scari, *Colloids Surf., A*, 2002, **211**, 43.
23 T. Y. Leung, C. Y. Chan, C. Hu, J. C. Yu and P. K. Wong, *Water Res.*, 2008, **42**, 4827.
24 R. M. Cornell and U. Schwertmann, *The Iron Oxides: Structure, Properties, Reactions, Occurrences, and Uses*, Wiley-VCH Verlag GmbH&Co., Weinheim, Germany, 2nd edn, 2003.

25 N. Lang, P. Delichere and A. Tuel, *Microporous Mesoporous Mater.*, 2002, **56**, 203.
26 H. D. Setiabudi, A. A. Jalil, S. Triwahyono, N. H. N. Kamarudin and R. R. Mukti, *Appl. Catal., A*, 2012, **417**, 190.
27 W. Cheng, S. Dong and E. Wang, *Langmuir*, 2003, **19**, 9434.
28 J. C. Groen, L. A. A. Peffer, J. A. Moulijn and J. Pérez-Ramírez, *Colloids Surf., A*, 2004, **241**, 53.
29 C. Dai, A. Zhang, L. Li, K. Hou, F. Ding, J. Li, D. Mu, C. Song, M. Liu and X. Guo, *Chem. Mater.*, 2013, **25**, 4197.
30 N. Sapawe, A. A. Jalil, S. Triwahyono, M. I. A. Shah, R. Jusoh, N. F. M. Salleh, B. H. Hameed and A. H. Karim, *Chem. Eng. J.*, 2013, **229**, 388.
31 B. Nikoobakht and M. A. El-Sayed, *Langmuir*, 2001, **17**, 6368.
32 S. Endud and K. L. Wong, *Microporous Mesoporous Mater.*, 2007, **101**, 256.
33 J. L. Bishop and E. Murad, *J. Raman Spectrosc.*, 2004, **35**, 480.
34 O. I. Peter, O. Chidi and M. A. Iheanacho, *Am. Chem. Sci. J.*, 2012, **2**, 45.
35 P. K. Jal, S. Patel and B. K. Mishra, *Talanta*, 2004, **62**, 1005.
36 Z. Xue, J. Ma, W. Hao, X. Bai, Y. Kang, J. Liu and R. Li, *J. Mater. Chem.*, 2012, **22**, 2532.
37 H. G. Karge, *Microporous Mesoporous Mater.*, 1998, **22**, 547.
38 H. Cong, R. Toftegaard, J. Arnbjerg and P. R. Ogilby, *Langmuir*, 2010, **26**, 4188.
39 C.-J. Jia and F. Schüth, *Phys. Chem. Chem. Phys.*, 2011, **13**, 2457.
40 J. C. Groen, G. M. Hamminga, J. A. Moulijn and J. Pérez-Ramírez, *Phys. Chem. Chem. Phys.*, 2007, **9**, 4822.
41 B. Li, K. Wu, T. Yuan, C. Han, J. Xu and X. Pang, *Microporous Mesoporous Mater.*, 2012, **151**, 277.
42 A. B. Bourlinos, M. A. Karakassides and D. Petridis, *J. Phys. Chem. B*, 2000, **104**, 4375.
43 P. Rieger, *Electron Spin Resonance*, Brown University, 1998.
44 R. D. Palma, S. Peeters, M. J. Van Bael, H. V. den Rul, K. Bonroy, W. Laureyn, J. Mullens, G. Borghs and G. Maes, *Chem. Mater.*, 2007, **19**, 1821.
45 M. E. Simonsen, C. Sønderby, Z. Li and E. G. Søgaard, *J. Mater. Sci.*, 2009, **44**, 2079.
46 C. Hariharan, *Appl. Catal., A*, 2006, **304**, 55.
47 W. Wang, Y. Yu, T. An, G. Li, H. Y. Yip, J. C. Yu and P. K. Wong, *Environ. Sci. Technol.*, 2012, **46**, 4599.
48 D. Zhang, *Acta Chim. Slovaca*, 2013, **6**, 141.
49 P. S. S. Kumar, M. R. Raj and S. Anandan, *Sol. Energy Mater. Sol. Cells*, 2010, **94**, 1783.
50 H. deLasa, B. Serrano and M. Salaices, *Photocatalytic Reaction Engineering*, Springer, New York, 2005.
51 A. Nezamzadeh-Ejhieh and G. Raja, *J. Chem.*, 2013, 685290.
52 N. Ferroudj, J. Nzimoto, A. Davidson, D. Talbot, E. Briot, V. Dupuisa, A. Bée, M. S. Medjramb and S. Abramson, *Appl. Catal., B*, 2013, **136**, 9.